

Towards a quantitative phase-field modeling of two-phase solidification

R. Folch* and M. Plapp

*Laboratoire de Physique de la Matière Condensée,
CNRS/École Polytechnique, 91128 Palaiseau, France*

(Dated: November 24, 2018)

We construct a diffuse-interface model of two-phase solidification that quantitatively reproduces the classic free boundary problem on solid-liquid interfaces in the thin-interface limit. Convergence tests and comparisons with boundary integral simulations of eutectic growth show good accuracy for steady-state lamellae, but the results for limit cycles depend on the interface thickness through the trijunction behavior. This raises the fundamental issue of diffuse multiple-junction dynamics.

PACS numbers: 64.70.Dv, 81.30.Fb, 05.70.Ln

Complex microstructures that arise during alloy solidification are a classical example of pattern formation [1] and influence the mechanical properties of the finished material [2]. A long-standing challenge is to understand the pattern selection starting from the basic ingredients: bulk transport, solute and heat rejection on the solidification front, and the local response of the interface. Since analytic solutions of this free-boundary problem (FBP) are rare, numerical modeling is mandatory.

The phase-field method [3] has become the method of choice for simulating solidification fronts [4], and more generally for tackling FBP and interfacial pattern formation phenomena, e.g. in materials science [5] and fluid flow [6]. Its main advantage is that it circumvents front tracking by using *phase fields* to locate the fronts. These fields interpolate between different constant values in each bulk phase through diffuse interfacial regions of thickness W . The model is required to reproduce the FBP in the sharp-interface limit, in which the extra length scale W vanishes.

In practice, simulations have to resolve the variation of the phase fields through the interfaces, so that W must stay finite. Their results generally depend on the ratio W/ℓ , where ℓ is a relevant length scale of the FBP. Explicit corrections to the original FBP to first order in W/ℓ have been calculated by a so-called *thin-interface* analysis in a few cases, and some canceled out [6, 7, 8, 9]. A complete cancellation has been achieved for single-phase solidification [7, 9], which means that results become independent of W/ℓ for some finite value of W . Accurate simulations of the correct FBP can then be run at that value, and it is possible to make *quantitative* contact between simulations, theory, and experiments in reasonable simulation times, as recently demonstrated for the dendritic solidification of a pure substance [10].

Here, we extend these advances to two-phase solidification, which already includes the most widespread solidification microstructures after dendrites: eutectic composites. They consist of alternate lamellae of two solids (α and β) or of rods of one solid embedded in the other, growing from a melt L near a eutectic point, where all three phases coexist at equilibrium. The interplay be-

tween capillarity and diffusive bulk transport between adjacent solid phases can give rise to more complex patterns and nonlinear phenomena such as bifurcations, limit cycles, solitary waves, and spatiotemporal chaos [11].

A two-phase solidification front consists of (i) solid-liquid interfaces and (ii) trijunction points where all three phases meet. Our strategy is to construct a phase-field model that allows us to analyze the thin-interface behavior of (i) separately from (ii); we thus quantitatively reproduce the correct FBP on the interfaces. At equilibrium, the trijunctions satisfy Young's law. We test convergence in W/ℓ for lamellar eutectic growth at experimentally relevant parameters, and compare our results to boundary integral (BI) [12] simulations and other phase-field models. For steady states, we achieve good agreement with the BI and a drastically improved, fast convergence compared to previous models. In contrast, the convergence is slow for limit cycles, due to the non-equilibrium behavior of the trijunctions, which affects the overall dynamics.

We use one phase field p_i to indicate presence ($p_i = 1$) or absence ($p_i = 0$) of each phase $i = \alpha, \beta, L$ in the spirit of volume fractions [13], which requires

$$p_\alpha + p_\beta + p_L = 1. \quad (1)$$

The phase fields evolve in time to minimize a free energy functional \mathcal{F} of $\vec{p} \equiv (p_\alpha, p_\beta, p_L)$, the solute concentration, and temperature,

$$\frac{\partial p_i}{\partial t} = -\frac{1}{\tau(\vec{p})} \frac{\delta \mathcal{F}}{\delta p_i} \bigg|_{p_\alpha + p_\beta + p_L = 1} \quad \forall i, \quad (2)$$

where $\tau(\vec{p})$ is a phase-dependent relaxation time. This classical problem of minimizing a functional subject to a constraint is treated by the method of Lagrange multipliers; $(\delta \mathcal{F} / \delta p_i)|_{p_\alpha + p_\beta + p_L = 1} = \delta \mathcal{F} / \delta p_i - (1/3) \sum_j \delta \mathcal{F} / \delta p_j$ for three phases, where the functional derivatives on the r.h.s. are now taken as if all p_i were independent.

To distinguish between phases, earlier phase-field models of two-phase solidification used either the usual solid-liquid phase field and the local concentration [14] or introduced a second, α - β phase field [15]. Across a solid-

liquid interface, both fields must vary, so that their dynamics are coupled, which complicates a thin-interface analysis. The same is true for a generic choice of \mathcal{F} in Eq. (2). However, if on an $i-j$ interface we can assure that the third phase field p_k is exactly zero, p_i or p_j can be eliminated using Eq. (1), so that the interface can be described in terms of a single independent variable. This was recently achieved using a free energy with cusp-like minima [16], but no thin-interface analysis is available for that model. We also achieve absence of the third phase, but using a *smooth* free energy, by requiring $p_k = 0$ to be a stable solution for p_k of Eqs. (2) for each $i-j$ interface:

$$\frac{\delta \mathcal{F}}{\delta p_k} \Big|_{p_\alpha + p_\beta + p_L = 1, p_k = 0} = 0 \quad \forall k, \quad (3a)$$

$$\frac{\delta^2 \mathcal{F}}{\delta p_k^2} \Big|_{p_\alpha + p_\beta + p_L = 1, p_k = 0} > 0 \quad \forall k. \quad (3b)$$

The advantage is that the simplest choice for \mathcal{F} yields a model that turns out to coincide with the quantitative model of Ref. [9] on those $i-j$ interfaces.

To construct our free energy, we split it into parts,

$$\mathcal{F} = \int_V f_{\text{grad}} + f_{\text{TW}} + \tilde{\lambda} f_c. \quad (4)$$

The first is a free energy penalty

$$f_{\text{grad}} = \frac{W^2}{2} \sum_i \left| \vec{\nabla} p_i \right|^2 \quad (5)$$

for the gradients of the phase fields that provides the interface thickness W . The next is a triple-well potential

$$f_{\text{TW}} = \sum_i p_i^2 (1 - p_i)^2 \quad (6)$$

that generates the “potential landscape”: one well per pure phase and “valleys” with double-well profiles along each $p_k = 0$ cut, separated by a potential barrier on trijunctions $p_\alpha = p_\beta = p_L = 1/3$. The last part has a strength $\tilde{\lambda}$ (a constant that controls convergence) and couples the phase fields p_i to the temperature T and the solute concentration C through $c(C) \equiv (C - C_E)/\Delta C$, where $\Delta C \equiv C_\beta - C_\alpha$, C_α and C_β are the limits of the eutectic plateau, and (C_E, T_E) is the eutectic point,

$$f_c = \sum_i g_i(\vec{p}) [B_i(T) - \mu A_i(T)], \quad (7)$$

where we have introduced the chemical-potential-like variable $\mu \equiv c - \sum_i A_i(T)h_i$, and $g_i(\vec{p})$ and $h_i(\vec{p})$ (given below) interpolate between 0 for $p_i = 0$ and 1 for $p_i = 1$.

The term f_c drives the system out of equilibrium by unbalancing the pure phase free energies: Each well i is shifted by an amount $B_i - \mu A_i$. The equilibrium value

$\mu = \mu_{\text{eq}}^{ij} = (B_j - B_i)/(A_j - A_i)$ gives equal shifts and hence restores the balance between phases i and j ; from the definition of μ , we obtain $c_i^{ij} = A_i + \mu_{\text{eq}}^{ij}$ for the concentration in phase i coexisting with phase j . A eutectic phase diagram with constant concentration gaps and straight liquidus and solidus lines is generated by $A_i = c_i \equiv c(C_i)$ and $B_i = c_i(T - T_E)/(m_i \Delta C)$, with m_i the (signed) liquidus slopes, $i = \alpha, \beta$. Non-constant concentration gaps and peritectic phase diagrams can also be treated. In all cases $A_L = B_L = 0$.

In order for $\mu = \mu_{\text{eq}}^{ij}$ to keep the balance all across the $i-j$ interface as p_i goes from 0 to 1, we require

$$g_i(p_i, p_j, 0) = 1 - g_i(p_j, p_i, 0) \quad \forall i. \quad (8)$$

Otherwise, several thin-interface corrections arise [8, 9]. The simplest choice satisfying also Eq. (3a) is $g_i = p_i^2 \{15(1 - p_i)[1 + p_i - (p_k - p_j)^2] + p_i(9p_i^2 - 5)\}/4$.

The evolution of μ is obtained from its definition and mass conservation, $\partial_t c + \vec{\nabla} \cdot \vec{J} = 0$, $\vec{J} = -Dp_L \vec{\nabla} \mu + \vec{J}_{\text{AT}}$:

$$\frac{\partial \mu}{\partial t} = D \vec{\nabla} \cdot (p_L \vec{\nabla} \mu) - \sum_i A_i \frac{\partial h_i}{\partial t} - \vec{\nabla} \cdot \vec{J}_{\text{AT}}, \quad (9)$$

where $-Dp_L \vec{\nabla} \mu$ is the usual diffusion current, with a diffusivity that varies from D in the liquid to 0 in the solid (one-sided model), and \vec{J}_{AT} is an extension of the anti-trapping current introduced in [9] that counterbalances spurious solute trapping,

$$\vec{J}_{\text{AT}} \equiv -\hat{n}_L \frac{W}{2\sqrt{2}} \sum_{i=\alpha, \beta} A_i \frac{\partial p_i}{\partial t} (\hat{n}_i \cdot \hat{n}_L), \quad (10)$$

where $\hat{n}_i = -\vec{\nabla} p_i / |\vec{\nabla} p_i|$ are unit vectors normal to $i-L$ interfaces, and $\hat{n}_i \cdot \hat{n}_L$ prevents solute exchange between the two solids. The model is not variational, because of the term \vec{J}_{AT} and because $\mu \neq \partial f_c / \partial c$, but enables us to use $h_i = p_i$, which allows for a coarser discretization [7].

Our model [Eqs. (2) and (9)] has stable interface solutions connecting two coexisting phases i and j : $\mu = \mu_{\text{eq}}^{ij}$, $p_i = 1 - p_j = \{1 \pm \tanh[r/(W\sqrt{2})]\}/2$ (with r the distance to the interface), $p_k = 0$. Since these solutions are identical for all $i-j$ pairs, so are the $i-j$ surface tensions. Unequal surface tensions can be obtained by adding new terms in Eq. (4) that shift the $i-j$ free energy barriers.

Remarkably, on solid-liquid ($i-L$) interfaces, assuming a weak dependence of the A_i , B_i on T , and $\tau(\vec{p}) = \tau_i$, the change of variables $\phi_i = p_i - p_L$, $u = (\mu_{\text{eq}}^{iL} - \mu)/A_i$ maps Eqs. (2) and (9) to the quantitative model with constant concentration gap in [9], up to numerical prefactors. The thin-interface limit can hence be deduced by inspection and yields the classic FBP on $i-L$ interfaces,

$$\partial_t c = D \nabla^2 c, \quad (11a)$$

$$-D \hat{n}_i \cdot \vec{\nabla} c = v_n (c_i^{iL} - c_L^{iL}), \quad (11b)$$

$$c = \mp \left(\frac{T - T_E}{|m_i| \Delta C} + d_i \kappa + \beta_i v_n \right), \quad (11c)$$

where Eq. (11a) holds in the liquid and the others are boundary conditions on the interface that has normal velocity v_n and curvature κ ; the minus (plus) refers to $i = \alpha$ (β), and the capillary lengths d_i and kinetic coefficients β_i read in terms of our model parameters

$$d_i = a_1 \frac{W}{|A_i|\tilde{\lambda}}, \quad (12)$$

$$\beta_i = a_1 \left[\frac{\tau_i}{|A_i|\tilde{\lambda}W} - a_2 \frac{|A_i|W}{D} \right], \quad (13)$$

with $a_1 = \sqrt{2}/3$ and $a_2 = 1.175$. The constant $\tilde{\lambda} \propto W/d_i$ in Eqs. (4), (12) and (13) controls the convergence to the original FBP. Any set of β_i can be treated with suitable τ_i . We consider here $\beta_\alpha = \beta_\beta = 0$, which is achieved with $\tau_i = a_2 A_i^2 \tilde{\lambda} W^2 / D$. The different τ_i for $A_\alpha \neq A_\beta$ (e.g. different concentration gaps) are interpolated by $\tau(\vec{p}) = \bar{\tau} + (1/2)(\tau_\alpha - \tau_\beta)(p_\alpha - p_\beta)/(p_\alpha + p_\beta)$, $\tau(p_\alpha + p_\beta = 0) = \bar{\tau}$, with $\bar{\tau} = (\tau_\alpha + \tau_\beta)/2$.

We test our model in directional solidification with $T = T_E + G(z - Vt)$, where $G > 0$ is the thermal gradient and $V > 0$, the pulling speed, both directed along the z axis. Half a eutectic lamellae pair of total width λ is simulated in two dimensions (x and z) with no-flux boundary conditions in the midline of each lamella, using a finite-difference Euler scheme with a grid spacing $\Delta x = 0.8W$ (coarser far into the liquid to improve efficiency). We adopt $l_D/\bar{d} = 51200$ and $\bar{l}_T/l_D = 4$, where $l_D \equiv D/V$ is the diffusion length, $l_T^i \equiv |m_i|\Delta c/G$ are the thermal lengths, and $\bar{d} \equiv (d_\alpha + d_\beta)/2$, $\bar{l}_T \equiv (l_T^\alpha + l_T^\beta)/2$. These correspond to typical experimental values $G \approx 100K/cm$, $V \approx 1\mu m/s$ for $\text{CBr}_4\text{-C}_2\text{Cl}_6$, an organic eutectic for which accurate experimental data exist [11]. We use $m_\alpha = -m_\beta$, $c_\alpha = -c_\beta$ (a symmetric phase diagram) or $m_\beta/m_\alpha = -2$, $-c_\beta/c_\alpha = d_\alpha/d_\beta = 2.5$ (one close to $\text{CBr}_4\text{-C}_2\text{Cl}_6$). In both cases $\mu(z \rightarrow +\infty) = 0$ (eutectic composition). We test convergence to the thin-interface limit with decreasing W by conversely increasing λ/W while keeping all the ratios above and λ/λ_{\min} fixed, where $\lambda_{\min} \propto \sqrt{d\bar{l}_D}$ is the minimal undercooling spacing [17]. This is achieved by varying the constant $\tilde{\lambda}$ in Eq. (12).

Figure 1 shows the solid-liquid interfaces of a steady-state lamellae pair calculated by different phase-field models and the boundary integral method [12] for $\lambda \approx \lambda_{\min}$. For the symmetric phase diagram [Fig. 1(a)], our model (thin solid lines) agrees well with the boundary integral (BI, thick solid line). Moreover, the curves at $\lambda/W = 92$ and 128 are indistinguishable from that at $\lambda/W = 64$. This means that the results are independent of λ/W for $\lambda/W > 64$, the signature of a quantitative model. In contrast, if we remove the antitrapping current in our model, $\vec{J}_{\text{AT}} = \vec{0}$, which leads to solute trapping and finite interface kinetics, the results depend on λ/W for all the range from 32 (bottom dashed line) to 128 (top one). The convergence of models not backed by a thin-interface analysis can even be slower, as shown by

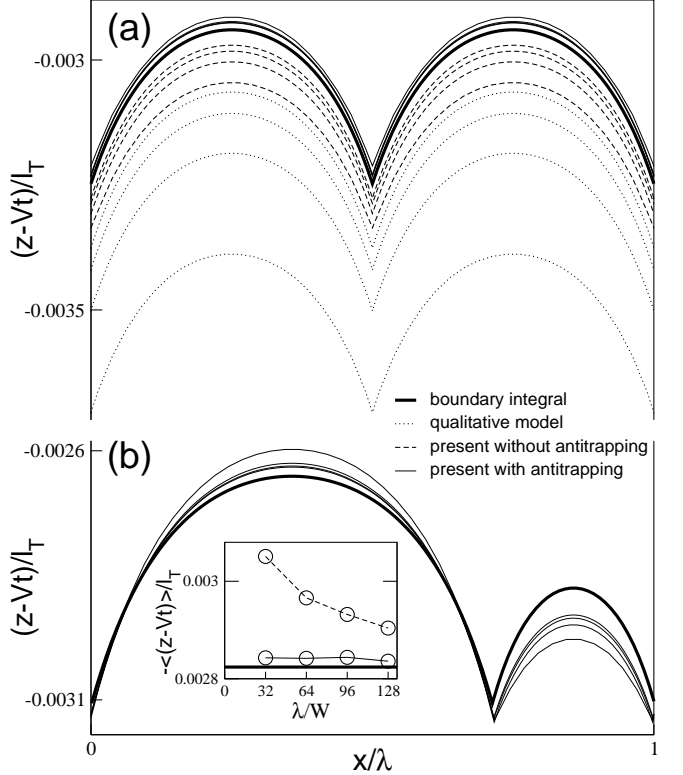


FIG. 1: Steady-state lamellae pair profiles (dimensionless undercooling *vs.* x/λ) for different models. Four curves at $\lambda/W = 32, 64, 96$ and 128 shown per model; curves closer to the boundary integral: larger λ/W . [$\lambda/W = 64\text{--}128$ collapse for the present model with antitrapping current in (a)]. Phase diagram used: (a) symmetric; (b) close to $\text{CBr}_4\text{-C}_2\text{Cl}_6$. See parameters in the text. Inset: Averaged undercooling in (b) *vs.* λ/W , compared to that without antitrapping current.

the dotted curves for a qualitative version of our model with $h_i = g_i$ violating Eq. (8) and $\vec{J}_{\text{AT}} = \vec{0}$ [18]; in this situation, several thin-interface corrections to the FBP occur simultaneously [8, 9].

Results are similar for the phase diagram close to $\text{CBr}_4\text{-C}_2\text{Cl}_6$ [Fig. 1(b)]. The convergence is somewhat slower, since one of the lamellae is thinner and needs to be properly resolved. Some small deviation from the BI persists, probably due to the trijunction behavior (see below). In the inset, we plot the average undercooling *vs.* λ/W . This is a less stringent test, as shown by the fact that results for our model are converged already for $\lambda/W = 32$. However, those for the model with $\vec{J}_{\text{AT}} = \vec{0}$ still depend on λ/W at $\lambda/W = 128$, which illustrates how all corrections need to be canceled before quantitative results can be achieved.

Next, we increase λ to $\approx 2.2\lambda_{\min}$, close above the threshold $\lambda \approx 2\lambda_{\min}$ [12] for the bifurcation from steady lamellae to oscillatory limit cycles, a situation in which the oscillation amplitude is very sensitive to all parameters. Indeed, for the symmetric phase diagram and $\lambda/W = 64$, the qualitative model of Ref. [18] still yields

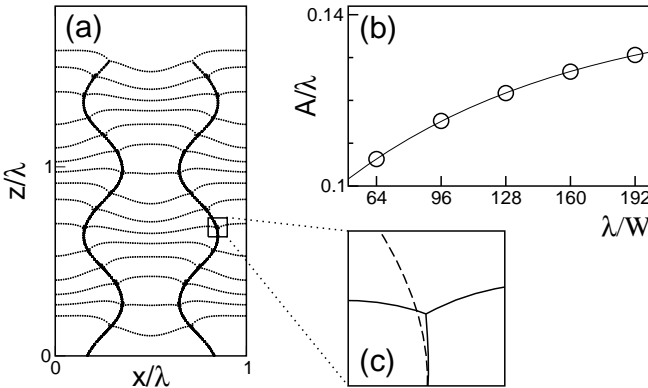


FIG. 2: Limit cycles. (a) Superimposed snapshots of the interfaces at constant time intervals for $\lambda/W = 64$. Thicker lines: α - β interfaces. (b) Amplitude of the trijunction oscillation in units of λ vs. λ/W . The line is a fit that yields $A(\lambda/W \rightarrow \infty)/\lambda = 0.142$. (c) Blowup of $6.4W \times 6.4W$. Solid lines: trijunction passage; dashed line: later α - β interface.

lamellae, whereas the present model correctly produces cycles, which are shown in Fig. 2(a). However, the amplitude of the trijunction oscillation A/λ , defined as its maximal displacement in x/λ , strongly depends on λ/W , as shown in Fig. 2(b). An extrapolation yields $A(\lambda/W \rightarrow \infty) = 0.142\lambda$, not far from the BI result $A = 0.139\lambda$, but the results are still not converged for $\lambda/W = 192$, in strong contrast to the steady-state behavior. This suggests that some correction(s) to the FBP in W/λ remain in our model. Since solid-liquid interfaces are controlled, we turn to the the trijunctions.

The solid (dashed) lines in Fig. 2(c) show a first (later) snapshot of the interfaces close to a turning point of the trijunction trajectory. In the later one the trijunction has moved away and only the α - β interface remains, which has slightly moved sideways. In the one-sided FBP, (i) the α - β interface *cannot* move, so it is the trace left by the trijunction, and (ii) its direction close to the trijunction approaches that of the trijunction velocity. In a diffuse-interface model, the diffusivity *behind* the $p_\alpha = p_\beta = p_L = 1/3$ trijunction point falls to zero on the scale of W , so that (i) and (ii) do not hold. We consistently observe the displacement to be a fraction of W fairly independent of λ/W , and the whole trijunction to be slightly rotated with respect to its velocity, features also observed for the steady state in Fig. 1b. This explains the remaining mismatch between phase-field and BI in Fig. 1b and the slow convergence of A/λ here.

In conclusion, we have presented a phase-field model of two-phase solidification that coincides with the best models to date [7, 9] on solid-liquid interfaces, whose dynamics are completely controlled. This has allowed us to identify the role of diffuse trijunctions in the convergence to the classic free-boundary problem.

Our results raise two interesting perspectives. First, it is clear that a thorough analysis of the multijunction

dynamics is needed before a fully quantitative modeling of multiphase solidification can be achieved. In the FBP, a trijunction is a singular point where the solidification front has an angle, and the solute current has a jump in magnitude and direction. Phase-field models smooth out these discontinuities, and only a particular way of smoothing can be expected to reduce to the FBP in the thin-interface limit. Second, the trijunction rotation was found to be fairly independent of the interface thickness. Since the physical interfaces are diffuse, this raises the question which description, FBP or diffuse-interface, is closer to nature. One promising way to elucidate this point could consist in the use of atomistic simulations.

We thank S. Akamatsu and G. Faivre for discussions, A. Karma for the BI code and Centre National d'Études Spatiales (France) for support.

* Present address: Universiteit Leiden, Postbus 9506, 2300 RA Leiden, The Netherlands.

- [1] E. Ben Jacob and H. Levine, *Adv. Phys.* **49**, 395 (2000); W. J. Boettinger *et al.* *Acta Mater.* **48**, 42 (2000).
- [2] W. Kurz and D. J. Fisher, *Fundamentals of Solidification* (Trans Tech, Aedermannsdorf, Switzerland, 1992).
- [3] J. S. Langer, in *Directions in Condensed Matter*, edited by G. Grinstein and G. Mazenko (World Scientific, Singapore, 1986), p. 164; J. B. Collins and H. Levine, *Phys. Rev. B* **31**, 6119 (1985); G. Caginalp and P. Fife, *Phys. Rev. B* **33**, 7792 (1986).
- [4] W. J. Boettinger, J. A. Warren, C. Beckermann and A. Karma, *Annu. Rev. Mater. Res.* **32**, 163 (2002).
- [5] L.-Q. Chen, *Annu. Rev. Mater. Res.* **32**, 113 (2002).
- [6] R. Folch, J. Casademunt, A. Hernández-Machado and L. Ramírez-Piscina, *Phys. Rev. E* **60**, 1724 (1999); **60**, 1734 (1999); T. Biben and C. Misbah, *Eur. Phys. J.* **29**, 311 (2002); *Phys. Rev. E* **67**, 031908 (2003).
- [7] A. Karma and W.-J. Rappel, *Phys. Rev. E* **53**, R3017 (1996); **57**, 4323 (1998).
- [8] R. F. Almgren, *SIAM J. Appl. Math.* **59**, 2086 (1999).
- [9] A. Karma, *Phys. Rev. Lett.* **87**, 115701 (2001); R. Folch, A. Karma, M. Plapp and B. Echebarria (unpublished).
- [10] J. Bragard, A. Karma, Y. H. Lee, and M. Plapp, *Interface Science* **10**, 121 (2002).
- [11] For instance M. Ginibre, S. Akamatsu, and G. Faivre, *Phys. Rev. E* **56**, 780 (1997).
- [12] A. Karma and A. Sarkissian, *Metall. Trans. A* **27**, 635 (1996);
- [13] I. Steinbach *et al.*, *Physica D* **94**, 135 (1996).
- [14] K. R. Elder, F. Drolet, J. M. Kosterlitz, and M. Grant, *Phys. Rev. Lett.* **72**, 677 (1994); A. Karma, *Phys. Rev. E* **49**, 2245 (1994).
- [15] A. A. Wheeler, G. B. McFadden, and W. J. Boettinger, *Proc. R. Soc. London, Ser. A* **452**, 495 (1996).
- [16] H. Garcke, B. Nestler, and B. Stoth, *SIAM J. Appl. Math.* **60**, 295 (1999).
- [17] K. A. Jackson and J. D. Hunt, *Trans. Metall. Soc. AIME* **236**, 1129 (1966).
- [18] R. Folch and M. Plapp, *cond-mat/0206237* (2002).